International Journal of Research
Available at https://edupediapublications.org/journals
e-ISSN: 2348-6848
p-ISSN: 2348-795X
Volume 05 Issue 12
April 2018

Bidirectional Single Stage Grid-Interactive Converter for Renewable energy applications

K. Mounika , T. Vigneysh , Dr.P.Sridhar

M-tech Student Scholar Department of Power Electronics and Electrical Drives, Institute of Aeronautical Engineering, Dundigal, Hyderabad, Telangana, India.
Email: kedam.mounika@gmail.com

Assistant Professor Department of Power Electronics and Electrical Drives, Institute of Aeronautical Engineering, Dundigal, Hyderabad, Telangana, India.
Email: t.vigneysh@iare.ac.in

Department of Power Electronics & Electrical Drives, (H.O.D) Institute of Aeronautical Engineering (IARE) , Dundigal, Hyderabad; Telangana, India
Email:Sridhar@iare.ac.in

Abstract: *In this concept PV-based stand-alone scheme for application in rural areas is proposed. Photovoltaic (PV) has become one of the most promising candidates among the available RESs. However, the availability of PV power is intermittent in nature, and hence, PV-based stand-alone systems need an energy storage element which is generally realized by utilizing a battery bank. Reformations in electricity sector along with various renewable energy promotion policies have increased the importance of small grid connected photovoltaic (PV) systems utilizing bidirectional single-stage grid-connected inverter (BSG inverter) for the battery energy storage system. This paper proposes BSG-inverter is composed of multiple bidirectional buck-boost type dc-dc converters (BBCs) and a dc-ac inverter for grid connected (PV) system. The output current of the inverter can be adjusted according to the voltage of the photovoltaic (PV) array. Advantages of the proposed BSG-inverter include: single-stage power conversion, low battery and dc-bus voltages, pulsating charging/discharging currents, and individual power control for each battery module.*

Keywords: DC–DC power converter, Batteries, Inverter, Photovoltaic cells

I. INTRODUCTION

Because of the fossil fuel exhaustion and global warming issue, renewable energies such as the photovoltaic (PV) power and wind turbines are more and more popular recently. However, the fluctuations of the high penetration renewable energy will cause the negative impact to the grid voltage and frequency stabilization. A battery energy storage system is a promising candidate to increase the penetration rate of the renewable energy. For the micro grid application, the battery energy storage system is essential not only for controlling and managing the energy of distributed generation units such as PVs, wind turbines, and micro turbines for the stability of the power system, but also for protecting loads from grid fault conditions.

As shown in Fig. 1, the conventional battery energy storage system consists of a battery array, which is formed by many battery modules connected in series or parallel, and a bidirectional grid-tied dc–ac inverter as a full-bridge inverter [1]–[3]. Circuit simplicity is the main advantage of this type of battery energy storage system but the total power capacity may be easily reduced by a particular overcharging/discharging battery module due to the battery tolerance, unequal battery losses, and so on.

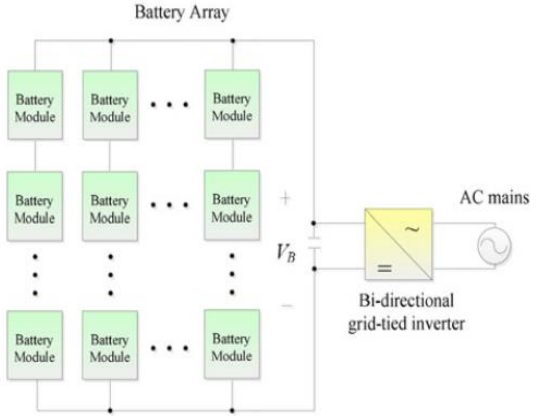

Fig 1: Conventional battery energy storage system.

In order to maximize energy storage, the voltage of the individual battery module connected in series to form a dc bus as the input of the grid-tied inverter must be equalized with each other. The general solution to solve the battery capacity reduction problem is to use extra balancing circuit to connect each battery module and balance the charge of all battery modules. However, the balancing circuit may result in the reduction of total efficiency and the increase of cost and circuit complexity.

Instead of using balancing circuit, Fig. 2 shows the different configurations of the grid-tied battery energy

International Journal of Research
Available at https://edupediapublications.org/journals
e-ISSN: 2348-6848
p-ISSN: 2348-795X
Volume 05 Issue 12
April 2018

storage system to balance the charge of all battery modules. A two-stage configuration to step up the voltage by a dc–dc converter and transfer the dc power into ac power by a dc–ac inverter is shown in Fig. 2(a) .Because of the parallel connection of each battery module, the equalization of battery modules can be naturally achieved. Also, the two stage configuration implies a simpler system design with lower control complexity. However, the high current stress of the dc–dc converter and an inverter as the second stage will reduce the overall conversion efficiency.

Thus, the power capacity of this type of configuration is limited due to the efficiency and the current stress considerations. An alternative configuration for the battery energy storage system is to adopt a dc–ac micro inverter for each battery module as shown in Fig. 2(b). Compared to the two-stage configuration, the micro inverter offers more flexibility and fault tolerance in the battery energy storage system.

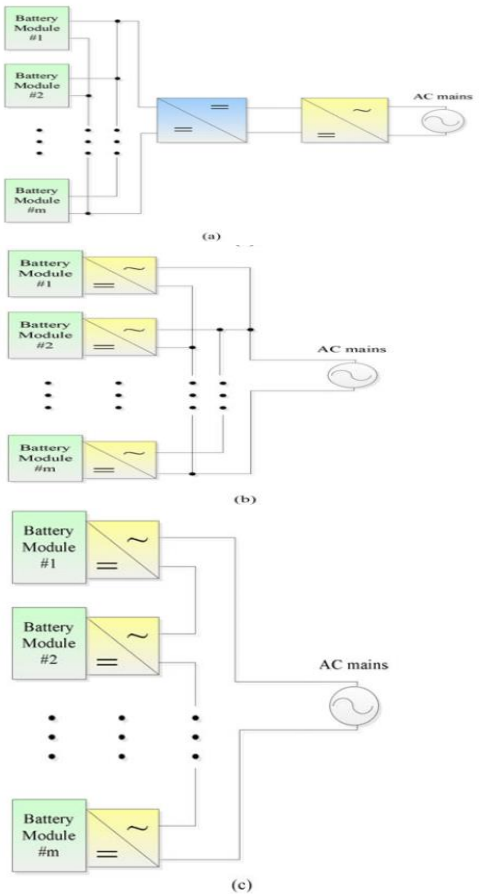

Fig 2: Different configurations of the battery energy storage system. (a) Two-stage configuration. (b) Micro inverter configuration. (c) Cascade-type configuration.

Since each battery module has its own grid-connected micro inverter, the output power of the battery module can be individually controlled in despite of other battery module mismatching. However, many challenges still remain in the way of achieving lower cost and higher conversion efficiency. Fig.2(c) shows the cascade-type configuration for the battery energy storage system where the output terminals of the inverter are connected in series. Since, low voltage rating components can be adopted with single-stage conversion, the inverter efficiency and cost can be improved. However, the control of those series-connected dc–ac inverters is complicated and the reliability of the battery storage system may be reduced.

Another key issue of the battery energy storage system is the life-time of the battery modules. Based on the power density and battery life consideration, the lead-acid battery and Li-ion battery are the most commonly used energy storage component for the battery energy storage system. However, the degradation of the electrochemical battery will affect the system's reliability dramatically. It has been reported that the sinusoidal current can improve the Li+ battery charging efficiency by comparing to the conventional constant-current constant voltage charging strategy.

Also, using pulsating currents to charge/discharge the electrochemical battery can improve the battery efficiency as well as increase the life-time of the battery. Conventionally, the battery energy storage system needs the two-stage converter to achieve the dc–ac function for the grid-connected inverter and to produce the pulsating charging/discharging current for the battery. Unfortunately, it will reduce the power conversion efficiency of the precious energy storage. Moreover, expensive current sensors are required to calculate the battery module output power for the output power control. Both the two-stage configuration and the expensive current sensor become the major barriers for the battery energy storage system. Therefore, a novel bidirectional single-stage grid-connected inverter (BSG-inverter) without using current sensors, as shown in Fig. 3, is proposed.

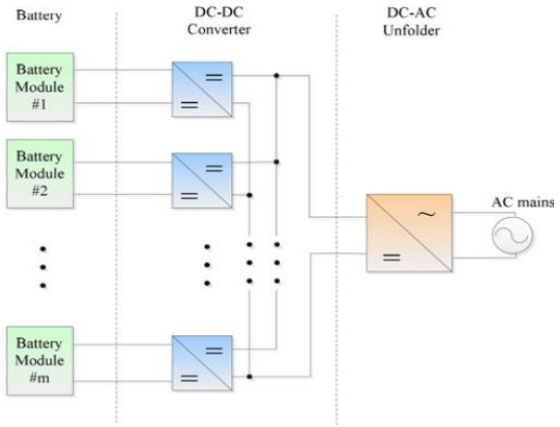

Fig 3: Proposed BSG-inverter for the battery energy storage system.

In Fig.3, each battery module has its own dc–dc converter to control the output power while the dc–ac inverter is realized by an output inductor and four active switches operated at ac line frequency. The dc–dc converter produces a high frequency pulsating dc current with a sinusoidal envelope. Therefore, low battery and dc-bus voltages can be accomplished. The pulsating charging/discharging current can help to extend the battery module's lifetime, too. The dc–ac inverter can convert the high frequency pulsating dc current generated by the dc–dc converters into a sinusoidal one with utility line frequency.

Because the inverter only switches at the zero crossing of the line voltage, its switching loss can be neglected by comparing to those power switches in the dc–dc converter. Therefore, the energy of each battery module is transferred to the ac mains by means of single-stage power conversion. Because of the single-stage operation, the power conversion efficiency can be improved. For the battery energy storage system, current sensors are always needed. Conventionally, two current sensors, one for the battery management system (BMS), which includes the state of charge and temperature monitoring, and the other for the power converter, which realizes the current control capability, are demanded for the battery energy storage system.

The proposed BSG-inverter can achieve the desired power flow control without the need of current sensors. Also, it can be adopted for different BMSs as long as the communication protocol for the power flow command is determined. The proposed BSG-inverter can improve the power conversion efficiency, reduce the output inductor size, eliminate the input current sensor, and simplify the control circuit. Moreover, the proposed BSG-inverter can achieve individual power control of each battery module so that important features of battery equalization, capacity flexibility, and hot swapping can be accomplished. In this paper, the operation principle of the BSG-inverter will be introduced and the power flow control of each battery module without current sensor will be developed. Computer simulation and preliminarily experiments are shown to verify the performance of the proposed BSG-inverter.

II. PROPOSED BSG-INVERTER

The circuit diagram of the proposed BSG-inverter, which is composed of m sets of distributed buck–boost type dc–dc converters (BBCs) and a dc–ac inverter, is shown in Fig. 3. Each BBC consists of two switches, two diodes, and one inductor. It can convert the dc current generated by the battery module into a high frequency pulsating dc current. This high frequency pulsating output current of the BBCs will be converted into sinusoidal one with utility line frequency by the dc–ac inverter of four active switches operated at low switching frequency and an LC filter. The proposed BSG-inverter will comply with the power commands, which is coming from the central control unit of the BMS, to charge or discharge the battery modules. The power flow from each battery module is transferred to the ac mains by means of single-stage power conversion. Also, the BBCs can be operated with interleaving to reduce the current ripple of the output inductor.

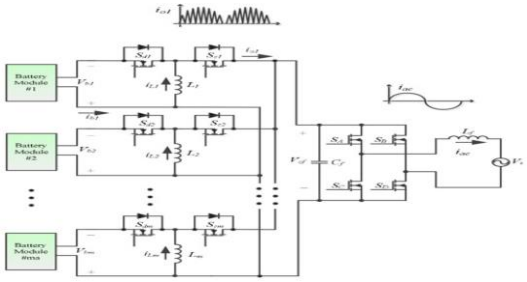

Fig 4: Circuit diagram of the proposed BSG-inverter

a) Discharging Mode Operation

For battery discharging mode of the first BBC set in Fig.4, the switch Sc1 is always turned off and the gate signal of Sd1 can be generated by comparing the rectified sinusoidal signal V_{sin} with the saw-tooth carrier signal V_{saw} with discontinuous current mode (DCM) operation as shown in Fig. 5(a). Because of the rectified sinusoidal pulse width modulation (SPWM) control with DCM operation, the waveform of the inductor current, iL1, has an envelope of the rectified ac mains. During the half-cycle of the grid line, the total switching numbers N can be expressed as follows:

$$N = \frac{f_s}{2f} \quad (1)$$

International Journal of Research
Available at https://edupediapublications.org/journals
e-ISSN: 2348-6848
p-ISSN: 2348-795X
Volume 05 Issue 12
April 2018

Where f_s is the switching frequency and f is the grid frequency. Typical waveforms of the inductor current, iL1, and output current, io1, for the DCM operation during the k^{th} switching cycle are shown in Fig. 5(b). In Fig. 5(b), id p1[k], dd1[k], and dd2[k] are defined as the peak current, the charging duty ratio, and the discharging duty ratio of the input inductor L1 of the k^{th} switching period Ts, respectively. For the first BBC set, during the charging period of the input inductor L1, the active switch Sd1 is turned on and the voltage potential across the input inductor L1 is equal to the battery voltage Vb1 which results in the linearly increased inductor current. When the switch Sd1 is turned off, the voltage potential across the input inductor L1 is reversed and equal to the capacitor voltage V_{cf} which can be assumed to be the rectified ac mains because of the dc–ac inverter. Due to the DCM operation,

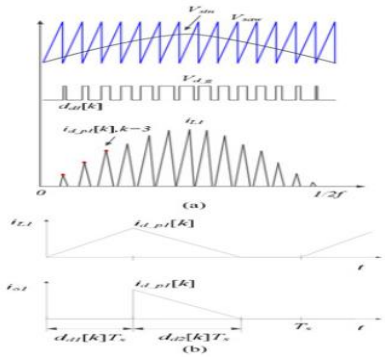

Fig 5: Control signal generation and input inductor current waveform of the first BBC in battery discharging mode. (a) Control signal generation.(b) Typical input inductor current and output current waveforms of the first BBC during the k^{th} switching cycle.

The inductor current iL1 decreases to zero during the discharging period of the input inductor L1. The peak current of the input inductor of the k^{th} switching cycle can be expressed as follows:

$$i_{d\_p1}[k] = \frac{V_{b1}}{L_1} \cdot d_{d1}[k]T_s = \frac{V_{cf}[k]}{L_1} \cdot d_{d2}[k]T_s \tag{2}$$

Where V_{cf} [k] is the output capacitor voltage during the k^{th} switching cycle. Due to the DCM SPWM control, (2) can be further modified as follows:

$$i_{d\_p1}[k] = \frac{V_{b1}}{L_1 f_s} \cdot D_{p1} \sin\left(\frac{k\pi}{N}\right) \tag{3}$$

Where Dp1 is the maximum duty ratio during the half-cycle of the grid line. To ensure the DCM operation in battery discharging mode, Dp1 must follow the following restriction:

$$D_{p1} < \left(\frac{\sqrt{2}V_{ac}}{V_{b1} + \sqrt{2}V_{ac}}\right) \tag{4}$$

where V_{ac} is the rms value of utility grid line voltage. It should be mentioned that the desired D p1 can be easily obtained by controlling the amplitude of the rectified sinusoidal signal V_{sin} as shown in Fig. 5(a). The average output current of the first BBC during the positive half-cycle can be derived as follows:

$$\langle i_{o1} \rangle = \frac{1}{N} \sum_{k=1}^{N} \frac{i_{d\_p1}[k] d_{d2}[k] T_s}{2}. \tag{5}$$

From (2) and (5), the average value of the output impedance of BBC can be expressed as follows:

$$\frac{\langle V_{cf} \rangle}{\langle i_{o1} \rangle} = \frac{1}{N} \sum_{k=1}^{N} \frac{2L_1 V_{cf}^2[k]}{V_{b1}^2 d_{d1}^2[k] T_s^2}. \tag{6}$$

In (6), the ratio of V_{cf} and dd1 for each k^{th} switching cycle can be approximated as a constant since both of them can be approximated as rectified sinusoidal functions. It implies that the BBC has a constant output impedance and can inject power into the ac mains with an almost unity power factor. Due to the DCM SPWM control with the current waveforms shown in Fig. 5(b), the average battery discharging power can be obtained as follows:

$$P_{b1} = \frac{V_{b1}}{2N} \sum_{k=1}^{N} i_{d\_p1}[k] d_{d1}[k]. \tag{7}$$

Combining (2), (3), and (7), the expression of the average battery discharging power becomes

$$P_{b1} = \frac{f}{L_1 f_s^2} \sum_{k=1}^{N} \left(V_{b1} D_{p1} \cdot \sin\left(\frac{k\pi}{N}\right)\right)^2. \tag{8}$$

Eq. (8) reveals that the average discharging power is only related to Vb1 and Dp1 if other parameters (f, fs, N, and L1) are carefully designed. In other words, the battery discharging power can be determined without measuring the battery current. By measuring the battery voltage Vb1 to generating appropriate maximum duty ratio Dp1 of the BBC, it is possible to realize the individual power-handling capability required for the battery energy storage system. Also, (8) implies that the variation of inductance value will affect the accuracy of the output power. It is similar to the situation that an imprecise current sensor will lead to an inaccurate output current control. Hence, it is necessary to calibrate the power calculation and determine the effective inductor value after the hardware circuit is implemented.

International Journal of Research
Available at https://edupediapublications.org/journals
e-ISSN: 2348-6848
p-ISSN: 2348-795X
Volume 05 Issue 12
April 2018

b) Charging Mode Operation

For battery charging mode of the first BBC set in Fig. 4, the switch Sd1 is always turned off and the gate signal of Sc1 can be generated by comparing the reference signal V_{ref} with the saw-tooth carrier signal V_{SAW} with DCM operation as shown in Fig. 6(a). In Fig. 6(b), d_{c1} is defined as the charging duty ratio of the input inductor L1 and $d_{c2}[k]$ is defined as the discharging duty ratio of the input inductor L1 of the k^{th} switching period Ts. For the first BBC set, during the charging period of the input inductor L1, the active switch Sc1 is turned on and the voltage potential across the input inductor L1 is equal to the capacitor voltage V_{cf} which can be assumed to be the rectified ac mains because of the dc–ac unfolder. When the switch Sc1 is turned off, the voltage potential across the input inductor L1 is reversed and equal to the battery voltage Vb1 which results in the linearly decreased inductor current. Due to the DCM operation, the inductor current iL1 decreases to zero during the discharging period. The peak current of the input inductor of the k^{th} switching cycle can be expressed as follows:

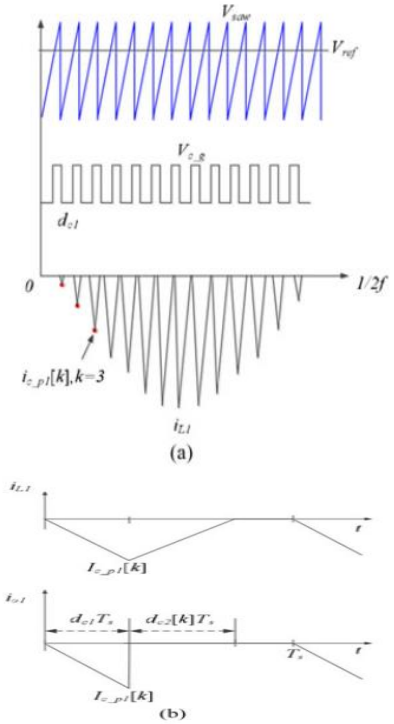

Fig 6: Control signal generation and input inductor current waveform of the first BBC in battery charging mode. (a) Control signal generation. (b) Typical input inductor current and output current waveforms of the first BBC during the kth switching cycle.

$$i_{c\_p1}[k] = -\frac{V_{cf}[k]}{L_1} \cdot d_{c1} T_s = \frac{V_{b1}}{L_1} \cdot d_{c2}[k] T_s. \quad (9)$$

Also, to ensure the DCM operation in battery charging mode, dc1 must follow the following restriction:

$$d_{c1} < \left(\frac{V_{b1}}{V_{b1} + \sqrt{2} V_{ac}} \right). \quad (10)$$

Due to the DCM SPWM control with the current waveforms shown in Fig. 6(b), the average battery charging power can be obtained as follows:

$$P_{b1} = \frac{f d_{c1}^2}{L_1 f_s^2} \sum_{k=1}^{N} (V_{cf}[k])^2. \quad (11)$$

Equation (3.11) reveals that the average battery charging power is only related to V_{cf} [k] and dc1 if other parameters (f_s, N, and L1) are carefully designed. Also, the battery charging power can be determined without measuring the battery current. The control block diagram of the first BBC set, as an example, is shown in Fig. 7. The discharging/charging and power commands, D/C and Pb1, are generated by the BMS and are sent to the controller of the BSG-inverter. The duty cycle signals, Dp1 and dc1, can be determined by using the derived (8) and (11). For the battery discharging operation, the unity sinusoidal function with the grid frequency, sinωt, can be via a phase-locked loop and is used to obtain the reference signal Dp1sinωt. The gate signal of Sd1 can be generated by comparing Dp1sinωt with the saw-tooth carrier signal V_{sw}. Also, the gate signal of Sc1 can be generated by comparing the duty cycle dc1 with the saw-tooth carrier signal V_{sw} for the battery charging operation.

The dc–ac unfolder is realized by four active switches operated at low switching frequency and an LC filter. It can convert the high frequency pulsating dc current generated by the BBCs into a sinusoidal one with utility line frequency. During the positive half-cycle of the ac mains, the switches SA and SD are turned-on while SB and SC are off. For the negative half-cycle, switches SB and SC are ON and SA and SD are OFF. Since the un folder is switched at the ac line frequency, its switching loss is very low and can be neglected. Therefore, the proposed BSG-inverter only has one high-frequency PWM signal and can be categorized as a single-stage inverter.

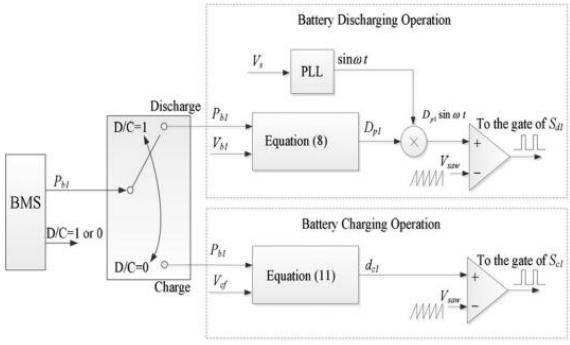

International Journal of Research
Available at https://edupediapublications.org/journals
e-ISSN: 2348-6848
p-ISSN: 2348-795X
Volume 05 Issue 12
April 2018

Fig 7: Control block diagram of the first BBC set.

For the proposed BSG-inverter, the m-sets of BBCs can operate in the interleaving fashion. The required synchronization signal for the interleaving operation can be easily obtained from the ac line voltage and no extra communication between BBC is required. By shifting the duty cycles of adjacent channels with 360°/m, the total current ripple of the output inductor can be greatly reduced. Fig. 8 shows the voltage and current waveforms of the BBC's output of two phase interleaving in battery discharging mode. The shifting time Tm of m-sets of BBCs can be expresses as follows:

$$T_m = \frac{1}{mf_s}. \tag{12}$$

Since the average voltage of output inductor Lf is zero at steady state, the average voltage across C_f is equal to V_{ac} and the peak discharging time T_{off} can be expressed as follows:

$$T_{\text{off}} = \frac{V_{b1}D_{p1}}{\sqrt{2}V_{\text{ac}}f_s}. \tag{13}$$

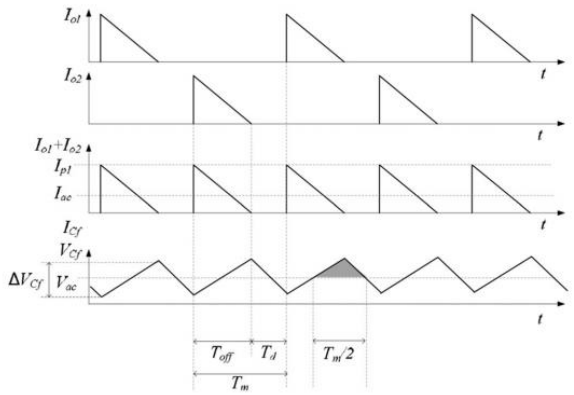

Fig 8: Output voltage and current waveforms of the BBC of two phase interleaving in battery discharging mode.

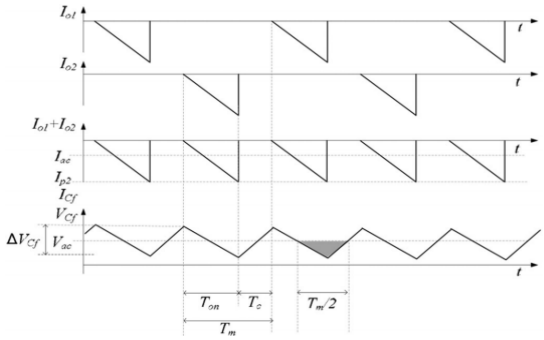

Fig 9: Output voltage and current waveforms of the BBC of two phase Interleaving in battery charging mode.

The discharging time of the capacitor C_f can be expressed as follows:

$$T_d = T_m - T_{\text{off}} = \frac{1}{mf_s} - \frac{V_{b1}D_{p1}}{\sqrt{2}V_s f_s}. \tag{14}$$

The peak voltage deviation of the output capacitor can be derived as follows:

$$\Delta V_{C_f} = \frac{T_d I_{\text{ac}}}{C_f} \tag{15}$$

Where, C_f is the capacitor value and I_{ac} is the peak value of the output current. Since the variation of the storage energy of the output capacitor is almost equal to the variation of the storage energy of the output inductor in Tm interval, the equation for the storage energy can be derived as follows:

$$E_d = \frac{1}{2}C_f \Delta V_{C_f}^2 = \frac{1}{2}L_f \Delta I_f^2 \tag{16}$$

where Lf is the output inductor value and ΔI_f is the peak current deviation of the output inductor. From (14)–(16), and Fig. 8, the peak current deviation of the output inductor can be obtained as follows:

$$\Delta I_f = \sqrt{\frac{\left(\frac{1}{mf_s} - \frac{V_{b1}D_{p1}}{\sqrt{2}V_s f_s}\right)^2 I_{\text{ac}}^2}{L_f C_f}}. \tag{17}$$

Fig. 9 shows the voltage and current waveforms of the BBC's output of two phases interleaving in charging mode. The average voltage across C_f must equal to V_{ac} and the charging time Ton can be expressed as follows:

$$T_{\text{on}} = \frac{d_{c1}}{f_s}. \tag{18}$$

The charging time of the capacitor C_f can be expressed as follows:

$$T_c = T_m - T_{\text{on}} = \frac{1}{mf_s} - \frac{d_{c1}}{f_s}. \tag{19}$$

The peak deviation of the output capacitor can be derived as follows:

$$\Delta V_{C_f} = \frac{T_c I_{\text{ac}}}{C_f}. \tag{20}$$

From (16), (19), (20), and Fig.8, the peak current deviation of the output inductor can be obtained as follows:

$$\Delta I_f = \sqrt{\frac{\left(\frac{1}{mf_s} - \frac{d_{c1}}{f_s}\right)^2 I_{ac}^2}{L_f C_f}}. \quad (21)$$

From (17) and (21), it can be found that the ripple current can be decreased by adding the numbers of the BBCs directly. This interleaved operation can result in lower ripple current to reduce the size of the output inductor and capacitor. Finally, the design procedure of the proposed BSG-inverter can be summarized as follows.

1) To ensure the DCM operation of the BBC, determine an eligible maximum duty ratio shown in (4) and (10) according to the rated voltage of the battery module and the ac mains.

2) Select the appropriate switching frequency and determine the total switching numbers shown in (1) with grid frequency.

3) Design the input inductor L1 shown in (8) and (11) with the circuit parameters f, f_s, D_{p1}, d_{c1}, N, and P_{b1}.

4) Based on the numbers of battery modules, shift the duty cycles of adjacent channels with 360°/m for the interleaving operation.

5) Select the appropriate value of the output current ripple to determine the output inductor and capacitor shown in (17) and (21) with the circuit parameters m, T_m , L_{p1}, L_1, V_s, and I_{ac}.

III PHOTOVOLTAIC TECHNOLOGY

A PV array consists of a number of PV modules, mounted in the same plane and electrically connected to give the required electrical output for the application. The PV array can be of any size from a few hundred watts to hundreds of kilowatts, although the larger systems are often divided into several electrically independent sub arrays each feeding into their own power conditioning system.

Photovoltaic's is the field of technology and research related to the devices which directly convert sunlight into electricity using semiconductors that exhibit the photovoltaic effect. Photovoltaic effect involves the creation of voltage in a material upon exposure to electromagnetic radiation.

The photovoltaic effect was first noted by a French physicist, Edmund Becquerel, in 1839, who found that certain materials would produce small amounts of electric current when exposed to light. In 1905, Albert Einstein described the nature of light and the photoelectric effect on which photovoltaic technology is based, for which he later won a Nobel Prize in physics. The first photovoltaic module was built by Bell Laboratories in 1954. It was billed as a solar battery and was mostly just a curiosity as it was too expensive to gain widespread use. In the 1960s, the space industry began to make the first serious use of the technology to provide power aboard spacecraft. Through the space programs, the technology advanced, its reliability was established, and the cost began to decline. During the energy crisis in the 1970s, photovoltaic technology gained recognition as a source of power for non-space applications.

The solar cell is the elementary building block of the photovoltaic technology. Solar cells are made of semiconductor materials, such as silicon. One of the properties of semiconductors that makes them most useful is that their conductivity may easily be modified by introducing impurities into their crystal lattice. For instance, in the fabrication of a photovoltaic solar cell, silicon, which has four valence electrons, is treated to increase its conductivity. On one side of the cell, the impurities, which are phosphorus atoms with five valence electrons (n-donor), donate weakly bound valence electrons to the silicon material, creating excess negative charge carriers.

On the other side, atoms of boron with three valence electrons (p-donor) create a greater affinity than silicon to attract electrons. Because the p-type silicon is in intimate contact with the n-type silicon a p-n junction is established and a diffusion of electrons occurs from the region of high electron concentration (the n-type side) into the region of low electron concentration (p-type side). When the electrons diffuse across the p-n junction, they recombine with holes on the p-type side.

However, the diffusion of carriers does not occur indefinitely, because the imbalance of charge immediately on either sides of the junction originates an electric field. This electric field forms a diode that promotes current to flow in only one direction.

Ohmic metal-semiconductor contacts are made to both the n-type and p-type sides of the solar cell, and the electrodes are ready to be connected to an external load. When photons of light fall on the cell, they transfer their energy to the charge carriers. The electric field across the junction separates photo-generated positive charge carriers (holes) from their negative counterpart (electrons). In this way an electrical current is extracted once the circuit is closed on an external load.

International Journal of Research
Available at https://edupediapublications.org/journals
e-ISSN: 2348-6848
p-ISSN: 2348-795X
Volume 05 Issue 12
April 2018

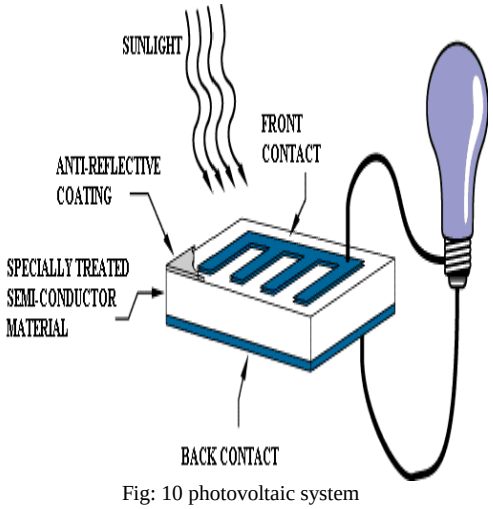

Fig: 10 photovoltaic system

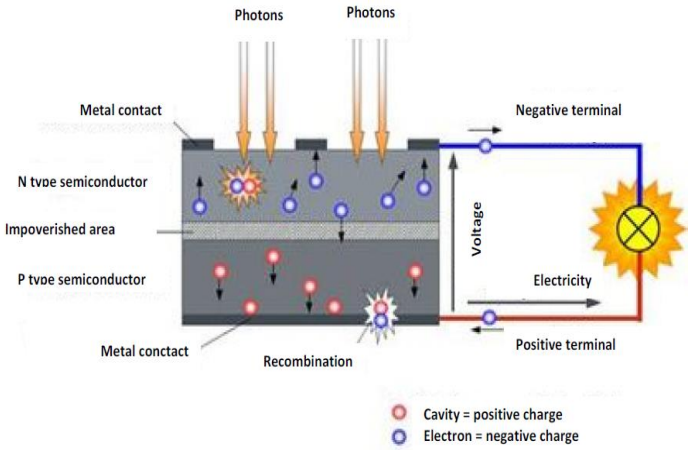

Fig 11: functioning of photovoltaic cells

A Functioning of the photovoltaic cells

The word "photovoltaic" consists of two words: photo, a Greek word for light, and voltaic, which defines the measurement value by which the activity of the electric field is expressed, i.e. the difference of potentials. Photovoltaic systems use cells to convert sunlight into electricity. Converting solar energy into electricity in a photovoltaic installation is the most known way of using solar energy.

The light has a dual character according to quantum physics. Light is a particle and it is a wave. The particles of light are called photons. Photons are mass less particles, moving at light speed. The energy of the photon depends on its wavelength and the frequency, and we can calculate it by the Einstein's law, which is:

$$E = hv$$

Where, E - photon energy, h - Planck's constant = $6.626\times10-34$Js

In metals and in the matter generally, electrons can exist as valence or as free. Valence electrons are associated with the atom, while the free electrons can move freely. In order for the valence electron to become free, he must get the energy that is greater than or equal to the energy of binding. Binding energy is the energy by which an electron is bound to an atom in one of the atomic bonds. In the case of photoelectric effect, the electron acquires the required energy by the collision with a photon. Part of the photon energy is consumed for the electron getting free from the influence of the atom which it is attached to, and the remaining energy is converted into kinetic energy of a now free electron. Free electrons obtained by the photoelectric effect are also called photoelectrons.

B. PV CELL MODEL

The equivalent circuit of a PV cell is shown in Fig 12. It includes a current source, a diode, a series resistance and a shunt resistance.

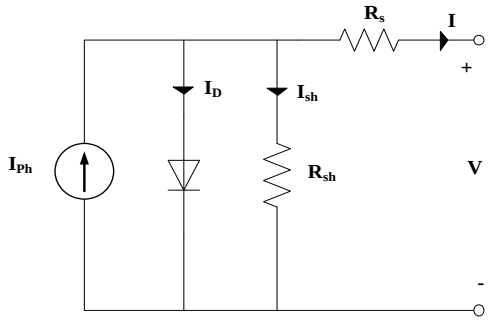

Fig. 12: PV cell equivalent circuit

In view of that, the current to the load can be given as:

$$I = I_{ph} - I_s(\exp\frac{q(V+R_sI)}{NKT}) -1) - \frac{(V+R_sI)}{R_{sh}} \quad (22)$$

In this equation, I_{ph} is the photocurrent, I_s is the reverse saturation current of the diode, q is the electron charge, V is the voltage across the diode, K is the Boltzmann's constant, T is the junction temperature, N is the ideality factor of the diode, and R_s and R_{sh} are the series and shunt resistors of the cell, respectively. As a result, the complete physical behavior of the PV cell is in relation with I_{ph}, I_s, R_s and R_{sh} from one hand and with two environmental parameters as the temperature and the solar radiation from the other hand.

International Journal of Research
Available at https://edupediapublications.org/journals
e-ISSN: 2348-6848
p-ISSN: 2348-795X
Volume 05 Issue 12
April 2018

SIMULATION RESULTS

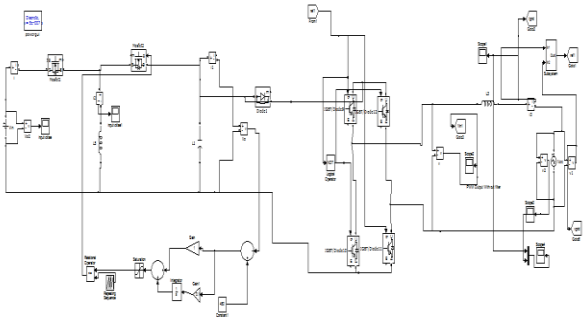

Fig 13: Battery charging mode

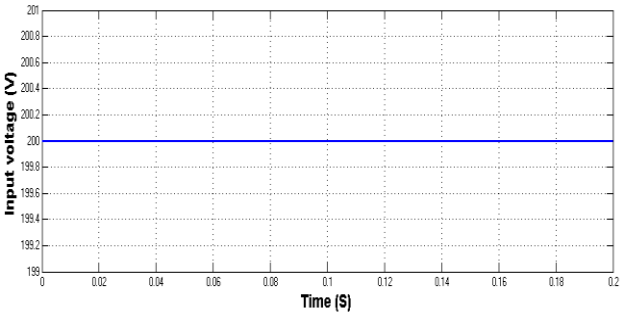

Fig 14: Battery input voltage

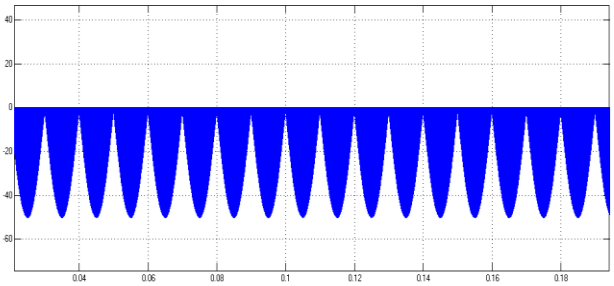

Fig 15: Inductor current in battery charging mode

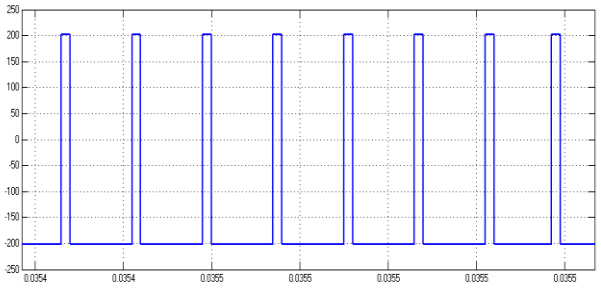

Fig 16: Inverter output voltage

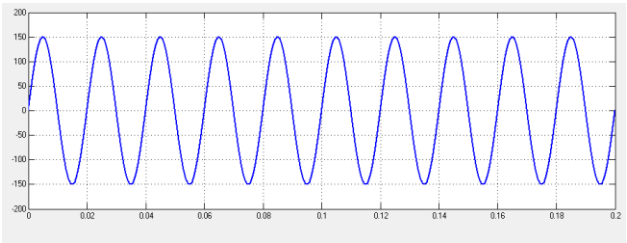

Fig 17: Grid voltage

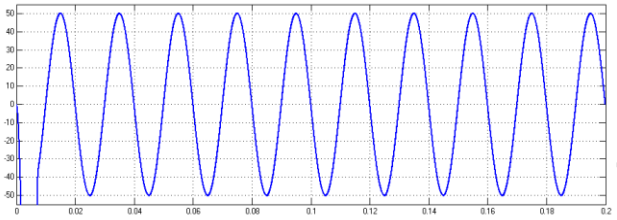

Fig 18: Grid current

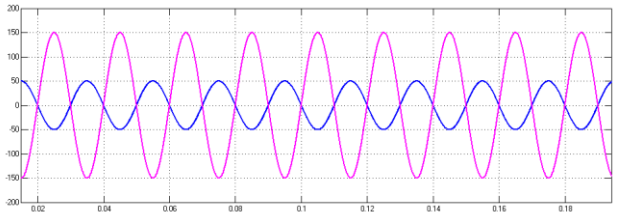

Fig 19: Grid voltage and current waveforms

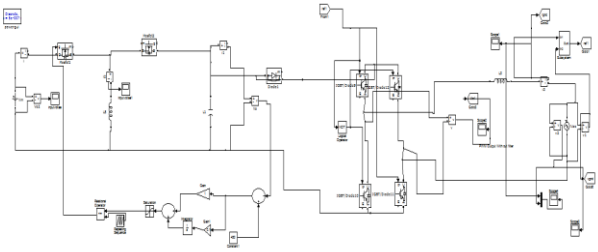

Fig 20: Battery discharging mode

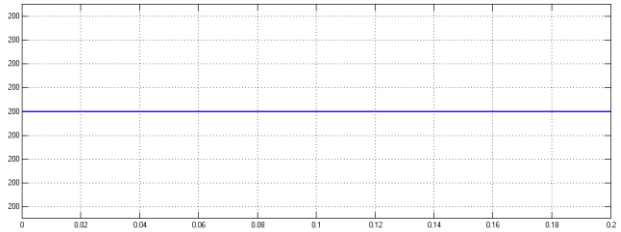

Fig 21: Battery input voltage

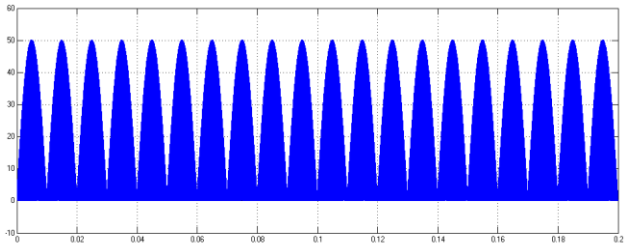

Fig 22: Inductor current

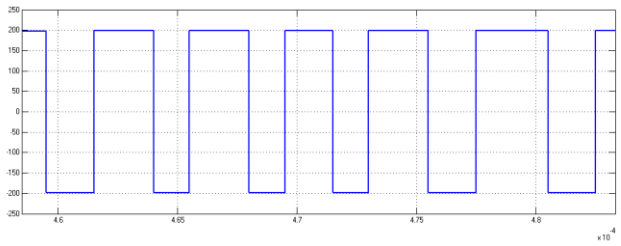

Fig 23: Inverter output voltage

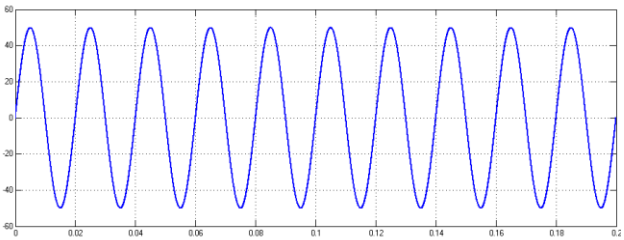

Fig 24: Grid voltage

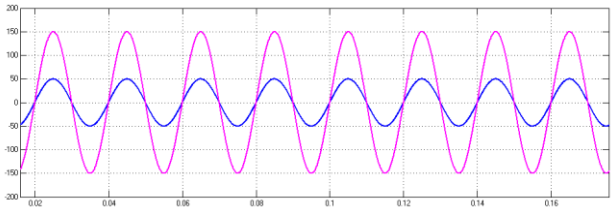

Fig 25: Grid voltage and current waveforms

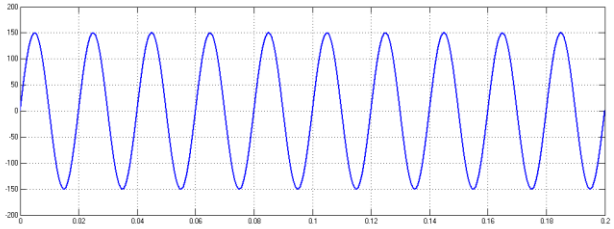

Fig 26: Grid current

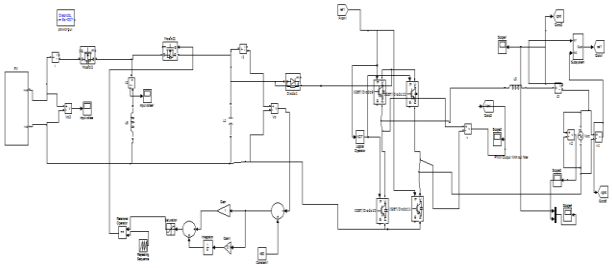

Fig 27: Photovoltaic cells

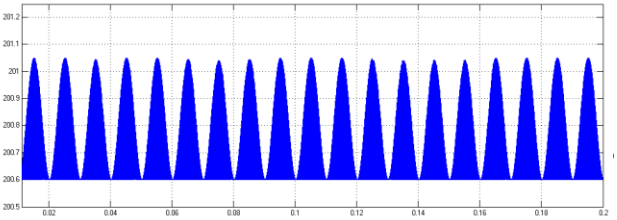

Fig 28: Photovoltaic cells Input voltage

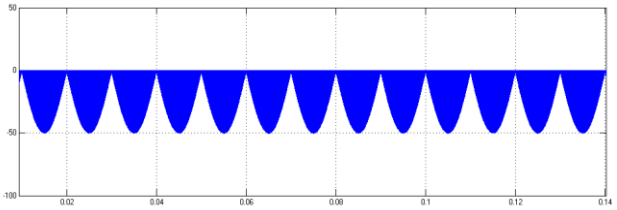

Fig 29: Inductor current

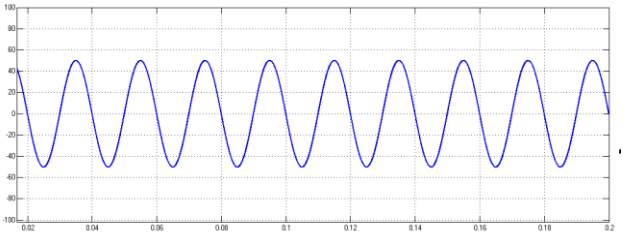

Fig 30: Grid current

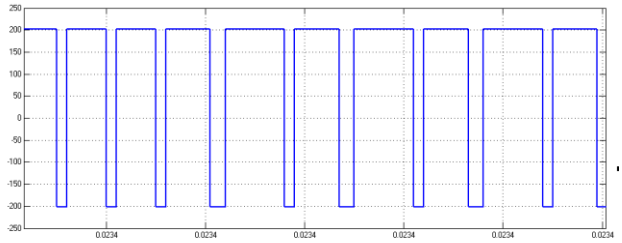

Fig 31: Inverter output voltage

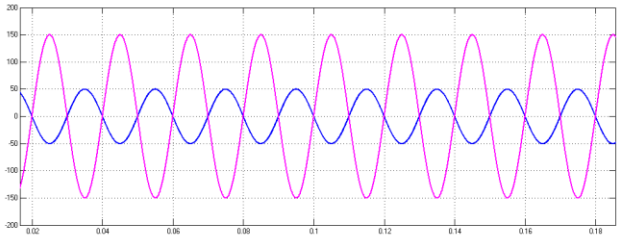

Fig 32: Grid voltage and current waveforms

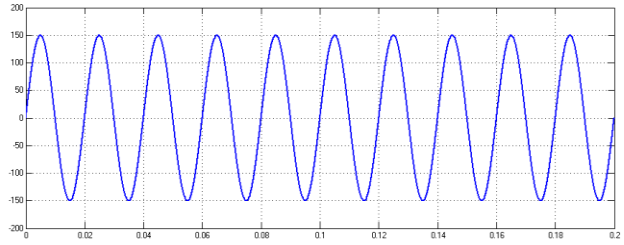

Fig 33: Grid voltage

IV CONCLUSION

A novel BSG-inverter, which consists of multiple distributed BBCs and a dc–ac unfolder, for the battery energy storage system has been proposed in this paper. The proposed BSG-inverter has individual power control capability for each battery module while fulfills the functions of battery charging and discharging by using pulsating current. Eventually, the equalization, lifetime extension, and capacity flexibility of the battery energy storage system can be achieved.

According to the developed mathematical equations, the power control capability of each individual battery module can be achieved without the need of input current sensor. Also, with the interleaved operation, the current ripple of the output inductor can be reduced significantly. A design guide line of the proposed BSG is presented. PV energy has grown rapidly in the last two decades and has become one of the most favorable distributed power generation systems based on renewable energy resources. Finally, computer simulations are shown to verify the validity of the proposed BSG-inverter & pv based inverter.

REFERENCES

[1] J. Y. Kim, J. H. Jeon, S. K. Kim, C. Cho, J. H. Park, H.-M. Kim, and K. Y. Nam, "Cooperative control strategy of energy storage system and microsources for stabilizing the microgrid during islanded operation," IEEE Trans. Power Electron., vol. 25, no. 12, pp. 3037 3048, Dec. 2010.
[2] H. Qian, J. Zhang, J. S. Lai, and W. Yu, "A high-efficiency grid-tie battery energy storage system," IEEE Trans. Power Electron., vol. 26, no. 3, pp. 886–896, Mar. 2011.
[3] J. He and Y. W. Li, "Hybrid voltage and current control approach for DGgrid interfacing converters with LCL filters," IEEE Trans. Ind. Electron., vol. 60, no. 5, pp. 1797–1809, Mar. 2013.
[4] M. Y. Kim, C. H. Kim, J. H. Kim, and G. W. Moon, "A chain structure of switched capacitor for improved cell balancing speed of lithium-ion batteries," IEEE Trans. Ind. Electron., vol. 61, no. 8, pp. 3989–3999, Aug. 2014.
[5] K. M. Lee, Y. H. Chung, C. H. Sung, and B. Kang, "Active cell balancing of Li-ion batteries using LC series resonant circuit," IEEE Trans. Ind. Electron., vol. 62, no. 9, pp. 5491–5501, Sep. 2015.
[6] W. Huang and A. Qahouq, "Energy sharing control scheme for stateof-charge balancing of distributed battery energy storage system," IEEE Trans. Ind. Electron., vol. 62, no. 5, pp. 2764–2776, May 2015.
[7] C. L. Chen, Y. Wang, J. S. Lai, and Y. S. Lee, "Design of parallel inverters for smooth mode transfer microgrid applications," IEEE Trans. Power Electron., vol. 25, no. 1, pp. 6–14, Jan. 2010.
[8] N. Mukherjee and D. Strickland, "Control of second-life hybrid battery energy storage system based on modular boost-multilevel buck converter," IEEE Trans. Ind. Electron., vol. 62, no. 2, pp. 1034–1046, Feb. 2015.
[9] H. Hu, S. Harb, N. H. Kutkt, Z. J. Shen, and I. Batarseh, "A single-stage microinverter without using electrolytic capacitors," IEEE Trans. Power Electron., vol. 28, no. 6, pp. 2677–2687, Jun. 2013.
[10] N. Sukesh, M. Pahlevaninezhad, and P. K. Jain, "Analysis and implementation of a single stage flyback PV microinverter with soft switching," IEEE Trans. Ind. Electron., vol. 61, no. 4, pp. 1819–1833, Apr. 2014.
[11] W. J. Cha, Y. W. Cho, and B. H. Kwon, "Highly efficient microinverter with soft-switching step-up converter and single-switch-modulation inverter," IEEE Trans. Ind. Electron., vol. 62, no. 6, pp. 3516–3523, Jun. 2015.
[12] L. Maharjan, T. Yamagishi, and H. Akagi, "Active-power control of individual converter cells for a battery energy storage system based on a multilevel cascade PWM converter," IEEE Trans. Power Electron., vol. 27, no. 3, pp. 1099–1107, Mar. 2012.
[13] M. Vasiladiotis and A. Rufer, "A modular multiport power electronic transformer with integrated split battery energy storage for versatile ultrafast EV charging stations," IEEE Trans. Ind. Electron., vol. 62, no. 5, pp. 3213–3222, May 2015.
[14] L. R. Chen, J. J. Chen, C. M. Ho, S. L. Wu, and D. T. Shieh, "Improvement of Li-ion battery discharging performance by pulse and sinusoidal current strategies," IEEE Trans. Ind. Electron., vol. 60, no. 12, pp. 5620–5628, Dec. 2013.
[15] L. R. Chen, S. L. Wu, D. T. Shieh, and T. R. Chen, "Sinusoidal-ripplecurrent charging strategy and optimal charging frequency study for Li-ion batteries," IEEE Trans. Ind. Electron., vol. 60, no. 1, pp. 88–97, Jan. 2013.
[16] J. Li, E. Murphy, J. Winnick, and P. A. Kohl, "The effects of pulse charging on cycling characteristics of commercial lithium-ion batteries," J. Power Sources, vol. 102, pp. 302–309, 2001.
[17] M. Liserre, F. Blaabjerg, and S. Hansen, "Design and control of an LCLfilter-based three phase active rectifier," IEEE Trans. Ind. Appl., vol. 41, no. 5, pp. 1281–1291, Sep./Oct. 2005.
[18] S. B. Kjaer, J. H. Pedersen, and F. Blaabjerg, "A review of singlephase grid-connected inverters for photovoltaic modules," IEEE Trans. Ind. Appl., vol. 41, no. 5, pp. 1292–1306, Sep. 2005.
[19] E. Koutroulis and F. Blaabjerg, "Design optimization of transformerless grid-connected PV inverters including reliability," IEEE Trans. Power Electron., vol. 28, no. 1, pp. 325–335, Jan. 2013.

[20] E. S. Sreeraj, K. Chatterjee, and S. Bandyopadhyay, "One-cycle-controlled single-stage single-phase voltage-sensorless grid-connected PV system," IEEE Trans. Ind. Electron., vol. 60, no. 3, pp. 1216–1224, Mar. 2013.
[21] Y. Tang, X. Dong, and Y. He, "Active buck-boost inverter," IEEE Trans. Ind. Electron., vol. 61, no. 9, pp. 4691–4697, Sep. 2014.
[22] H. R. Teymour, D. Sutanto, K. M. Muttaqi, and P. Ciufo, "Solar PV and battery storage integration using a new configuration of a three-level NPC inverter with advanced control strategy," IEEE Trans. Energy Convers., vol. 29, no. 2, pp. 354–365, Jun. 2014.
[23] W. Li, Y. Gu, H. Luo, W. Cui, X. He, and C. Xia, "Topology review and derivation methodology of single-phase transformerless photovoltaic inverters for leakage current suppression," IEEE Trans. Ind. Electron., vol. 62, no. 7, pp. 4537–4551, Jul. 2015.
[24] S. Poshtkouhi, V. Palaniappan, and O. Trescases, "A general approach for quantifying the benefit of distributed power electronics for fine grained MPPT in photovoltaic applications using 3-D modeling," IEEE Trans. Power Electron., vol. 27, no. 11, pp. 4656–4666, Nov. 2012.
[25] N. Kasa, T. Iida, and L. Chen, "Flyback inverter controlled by sensorless current MPPT for photovoltaic power system," IEEE Trans. Ind. Electron., vol. 52, no. 4, pp. 1145–1152, Aug. 2005.
[26] Y. M. Chen, K. Y. Lo, and Y. R. Chang, "Multi-string single-stage gridconnected inverter for PV system," in Proc. Energy Convers. Congr. Expo., 2011, pp. 2751–2756.
[27] H. Patel and V. Agarwal, "A single-stage single-phase transformer-less doubly grounded grid-connected PV interface," IEEE Trans. Energy Convers., vol. 24, no. 1, pp. 93–101, Mar. 2009.
[28] F. Tian, S. Kasemsan, and I. Batarseh, "An adaptive slope compensation for the single-stage inverter with peak current-mode control," IEEE Trans. Power Electron., vol. 26, no. 10, pp. 2857–2862, Oct. 2011.

AUTHOR DETAILS

Author - 1
K. Mounika
M-tech Student Scholar
Department of Power Electronics and Electrical Drives,
Institute of Aeronautical Engineering, Dundigal,
Hyderabad, Telangana, India.
Email: kedam.mounika@gmail.com

Interested Areas – Power Electronics

Author - 2

T. Vigneysh
Assistant Professor
Department of Electrical & Electronics Engineering,
Institute of Aeronautical Engineering, Dundigal,
Hyderabad, Telangana, India.
Email: t.vigneysh@iare.ac.in

Author – 3
P. Sridhar
Professor (H.O.D)
Department of Electrical & Electronics Engineering,
Institute of Aeronautical Engineering, Dundigal,
Hyderabad, Telangana, India.
Email: sridhar@iare.ac.in